



**HAL**  
open science

## Water transport properties of thermoplastic polyurethane films

N. Dolmaire, Éliane Espuche, Françoise Méchin, J.-P. Pascault

► **To cite this version:**

N. Dolmaire, Éliane Espuche, Françoise Méchin, J.-P. Pascault. Water transport properties of thermoplastic polyurethane films. *Journal of Polymer Science Part B: Polymer Physics*, 2004, 42 (3), pp.473-492. 10.1002/polb.10716 . hal-02057693

**HAL Id: hal-02057693**

**<https://hal.science/hal-02057693>**

Submitted on 22 Feb 2022

**HAL** is a multi-disciplinary open access archive for the deposit and dissemination of scientific research documents, whether they are published or not. The documents may come from teaching and research institutions in France or abroad, or from public or private research centers.

L'archive ouverte pluridisciplinaire **HAL**, est destinée au dépôt et à la diffusion de documents scientifiques de niveau recherche, publiés ou non, émanant des établissements d'enseignement et de recherche français ou étrangers, des laboratoires publics ou privés.

## Water Transport Properties of Thermoplastic Polyurethane Films

N. DOLMAIRE,<sup>1,2</sup> E. ESPUCHE,<sup>1</sup> F. MÉCHIN,<sup>2</sup> J.-P. PASCAULT<sup>2</sup>

<sup>1</sup>Laboratoire des Matériaux Polymères et des Biomatériaux, Unité mixte de recherche (UMR) Centre National de la Recherche Scientifique (CNRS) 5627 Ingénierie des Matériaux Polymères (IMP), Bât. ISTIL, Université Claude Bernard 43, Bd. du 11 Novembre 1918, 69622 Villeurbanne Cedex, France

<sup>2</sup>Laboratoire des Matériaux Macromoléculaires, UMR CNRS 5627 IMP, Institut National des Sciences Appliquées, 20, Ave A. Einstein, 69621 Villeurbanne Cedex, France

**ABSTRACT:** Two linear segmented polyurethanes, based on poly(oxyethylene) (POE) as a soft segment and 4,4'-diphenylmethane diisocyanate and 1,4-butanediol as hard segments and differing in their soft segment length, have been studied from a water vapor transport point of view. For both polyurethanes, the water sorption is governed by a Fickian process, and the thermoplastic polyurethane with the longer POE segments displays the higher water diffusion rate. The water sorption isotherms are Brunauer Emmet Teller (BET) type III for both thermoplastic polyurethanes, and the water uptakes are directly related to the polymer POE content. The Flory–Huggins theory cannot correctly describe the sorption isotherms. More sophisticated approaches (Koningsveld–Kleinjens or Guggenheim–Anderson–de Boer (GAB) models) are needed to fit the experimental water uptakes. The positive deviation from Henry's law and the decrease in the apparent diffusion coefficient observed at a high activity have been particularly studied. In this activity range, an isotherm analysis based on the cluster integral of Zimm and Lundberg suggests some clustering phenomenon, which seems consistent with the diffusion coefficient variation. In agreement with the sorption results, the water permeability coefficients are small at low activities, and they increase greatly with the relative pressure of water.

**Keywords:** polyurethanes; water sorption; diffusion; water clustering; water permeation; structure-property relations

## INTRODUCTION

Hydration properties are very important for many applications, such as biocompatible materials, barrier materials, packaging, breathable materials, and membrane separation processes. Linear segmented polyurethanes have been developed for many of these domains, but in comparison with other families of synthetic polymers, relatively little attention has been paid to the study of their hydration mechanisms (1-7). In particular, most studies have established structure–transport property relationships that consider only liquid water sorption properties (6,7). For breathable material applications, the analysis of the water vapor flow ( $J$ ) must be considered. These applications require a high flow associated with fast diffusion, whatever the water vapor pressure gradient is. For hydrophilic polymers, which are often used to realize dense breathable membranes,  $J$  is controlled by a solution-diffusion mechanism: diffusion, permeation, and solubility are thus closely related. Furthermore, the evolution of these three transport factors as a function of the activity is usually a nonideal process. At a high activity, complex diffusion mechanisms are often observed, and they are related to complex water sorption isotherms. Deviations from Henry's law are frequently noticed at high relative humidities (8,9) because of plasticization or water clustering (10,11).

In this work, the water vapor transport mechanisms of two commercial hydrophilic thermoplastic polyurethanes (TPUs) were studied. To establish structure–transport property relationships, we identified the chemical structures of the TPUs and determined their physicochemical properties. The kinetics and equilibria of water vapor sorption were studied over the entire range of water activity ( $a_w$ ), and the efficiencies of different models in describing the sorption isotherms were evaluated. Both kinetic and equilibria sorption results allowed us to propose a sorption mechanism in which the participation of a water clustering phenomenon was clearly identified and analyzed.

The water vapor permeation properties were also studied as a function of the partial pressure and were related to the water vapor sorption mechanism.

A better understanding of the transport properties of these TPU reference materials allows us to envision their future modification to better adapt their properties to the desired applications.

## EXPERIMENTAL

### Materials

The two polyurethanes (TPUs) studied, Estane 58237 and Estane 58245, were provided by Noveon.

The number-average molecular weights ( $\overline{M}_n$ 's) and weight-average molecular weights ( $\overline{M}_w$ 's) of the raw TPUs were evaluated by size exclusion chromatography in tetrahydrofuran (THF; 1 mL/min) with a Viscotek chromatograph equipped with a VE1121 pump, a VE5111 injector, and a VE3580 refractometer and with three Styragel HR 5E columns (Waters) in series. The values (with respect to a polystyrene calibration) were  $\overline{M}_n = 26,000 \pm 2000$  and  $\overline{M}_w = 86,000 \pm 4000$  for Estane 58237 ( $\overline{M}_w/\overline{M}_n = 3.3$ ) and  $\overline{M}_n = 37,000 \pm 2000$  and  $\overline{M}_w = 72,000 \pm 4000$  for Estane 58245 ( $\overline{M}_w/\overline{M}_n = 2.0$ ). The chromatograms are depicted in Figure 1. To understand the TPU transport properties and to have better control over the future grafting reactions, we tried at first to obtain a precise image of the chemical structure of this material, using Fourier transform infrared spectroscopy and mainly  $^1\text{H}$  and  $^{13}\text{C}$  NMR (Fig. 2).

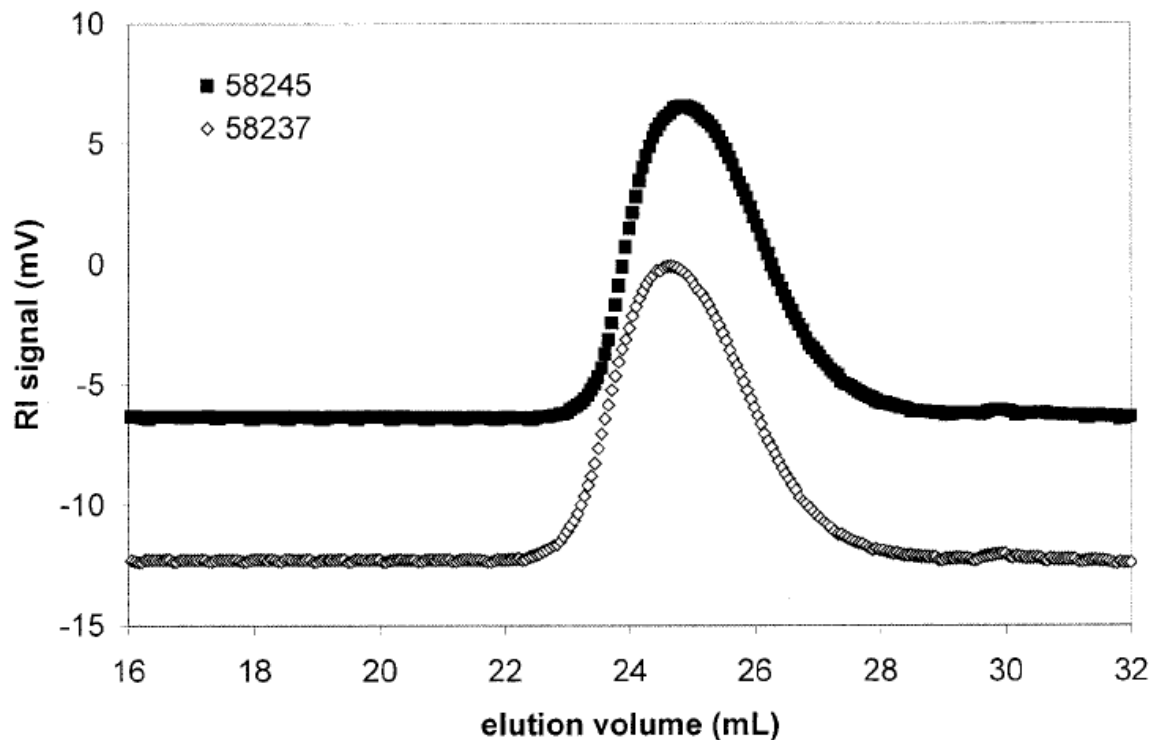


**Figure 1.** Size exclusion chromatography traces (THF and 25 °C) of Estane 58237 and Estane 58245.

From these analyses, we concluded that the soft segments were based on poly(oxyethylene) (POE), whereas 4,4'-diphenylmethane diisocyanate (MDI) extended with 1,4-butanediol (BDO) was used to yield the hard segments. The composition could thus be expressed as POE/MDI/BDO (1/1 +  $x/x$ ; the calculations are discussed later). More precisely, the peak integrations of the  $^1\text{H}$  spectrum [Fig. 2(a)] were compatible with the structure depicted in Figure 3 and their corresponding attributions indicated in Table 1. From these data, it was possible to determine separately the lengths of the soft (parameter  $n$ ) and hard (parameter  $x$ ) segments; we found the following average values (rejecting the peak associated with the urethane NH group): Estane 58237,  $n \approx 21.5$  and  $x \approx 2.34$ , and Estane 58245,  $n \approx 33.3$  and  $x \approx 2.74$ .

The data determined from  $^{13}\text{C}$  analysis, obtained under quantitative conditions [Estane 58237; Fig. 2(b) and Table 2], are in complete agreement with these results. With  $^1\text{H}$  values, several characteristic features for the starting TPU can be deduced:

1. The average molar mass of the initial POE used as the soft segment in each TPU ( $44n + 18$ ): approximately 1000 g/mol for Estane 58237 and approximately 1500 g/mol for Estane 58245.
2. The overall POE weight proportion in both TPUs (equal to  $(44n + 18)/(44n + 340x + 268)$ , according to the composition indicated previously): 48.0 wt % in Estane 58237 (corresponding to 52.0 wt % MDI–BDO hard segments) and 55.7 wt % in Estane 58245 (corresponding to 44.3 wt % hard segments).
3. The urethane equivalent weight (or the average molar mass per urethane bond, being equal to  $(44n + 340x + 268)/(2x + 2)$ , according to the composition indicated previously): 301 g.mol $^{-1}$  for Estane 58237 and 356 g.mol $^{-1}$  for Estane 58245 (i.e., the average number of urethane bonds per chain is about 90 for 58237 and 105 for 58245, according to polystyrene standards).

From these results, it is easy to understand why Estane 58245 is generally said to be more breathable than the other TPU because it displays longer POE segments and contains higher amounts of this hydrophilic moiety. In the text, Estane 58245 will be called PU55 and Estane 58237 PU48 in reference to the percentage of POE.

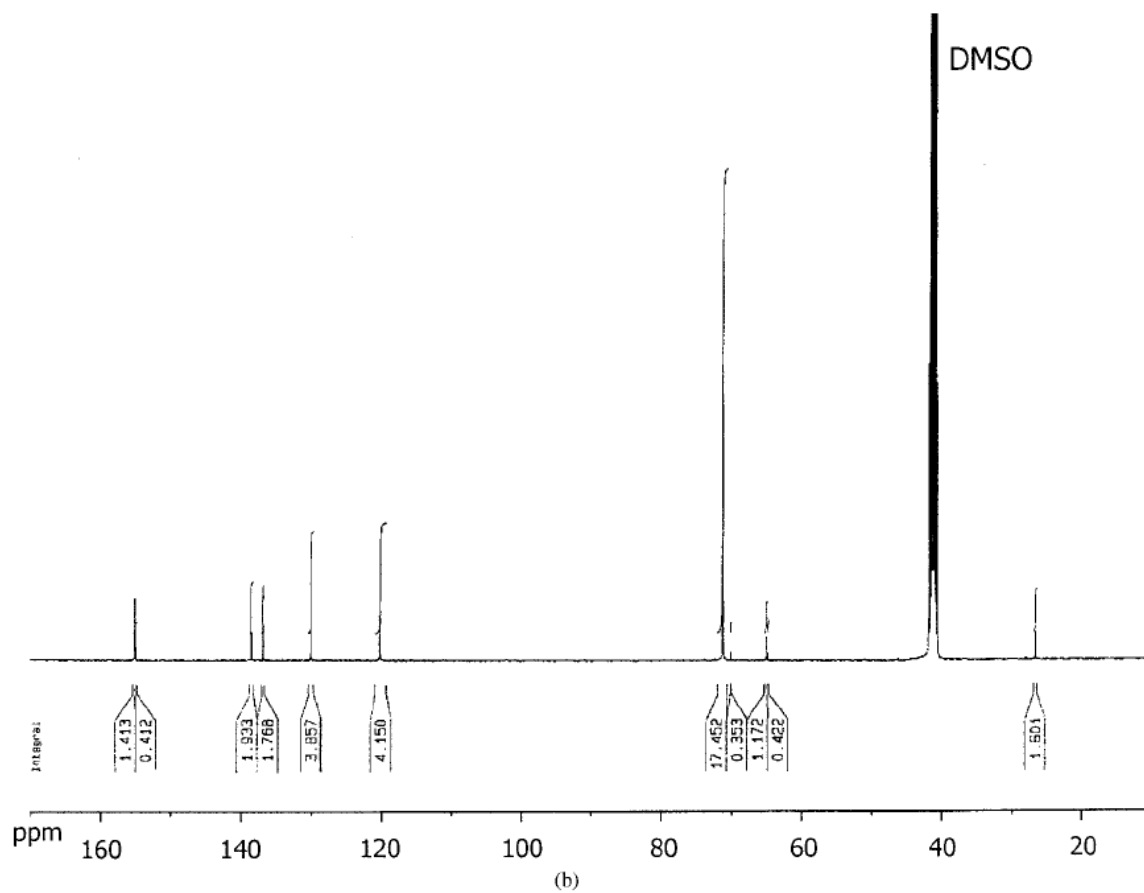
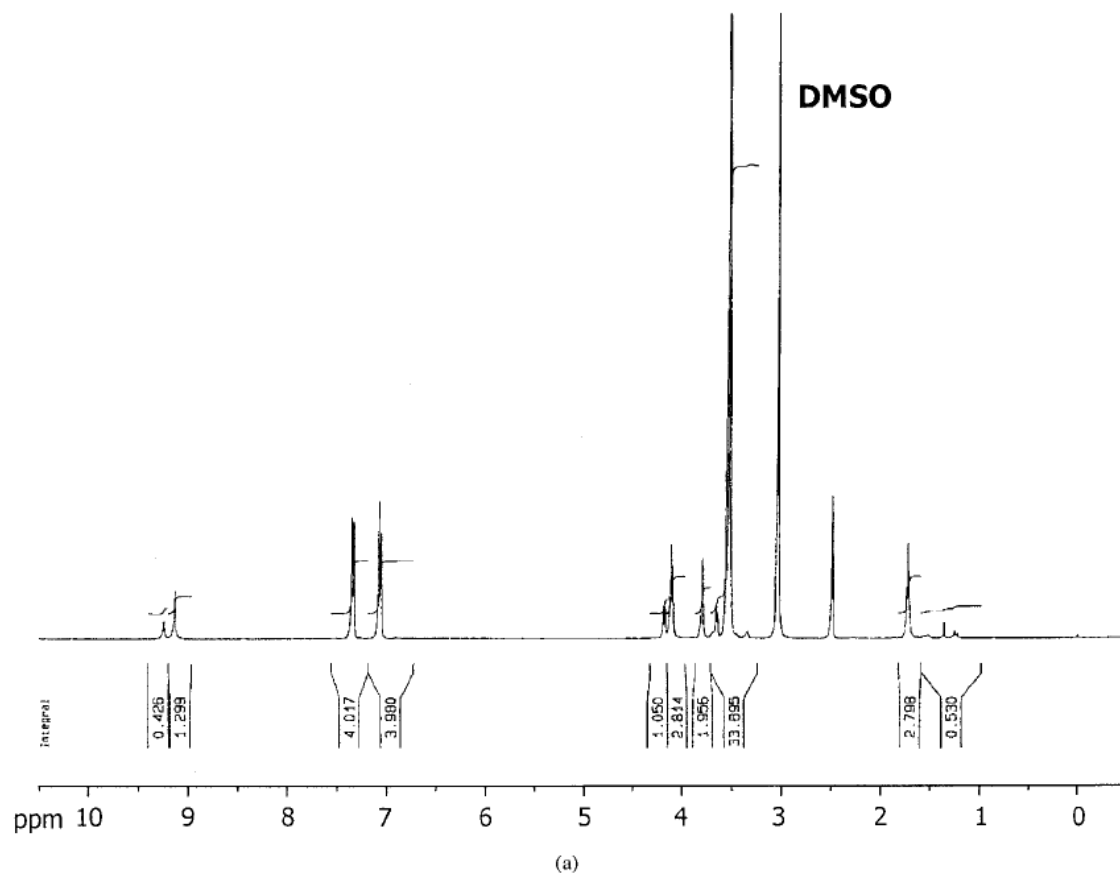
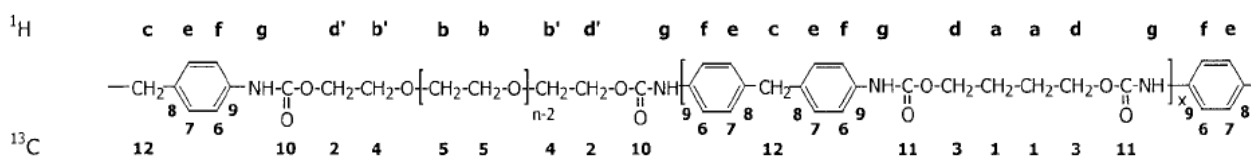


Figure 2. (a)  $^1\text{H}$  NMR and (b)  $^{13}\text{C}$  NMR spectra of Estane 58245.



**Figure 3.** TPU structure.

### Film Process

TPU films were prepared by two methods. The first one consisted of casting a solution containing 1 wt % TPU dissolved in THF on a glass plate. After the solution dried *in vacuo* at 40 °C for 1 h, 40 μm-thick films were obtained, and they were placed in an oven for 2 h at 40 °C. The second method was a solvent-free process. It was used to prepare PU55 films. The method consisted of the coextrusion and blowing of a three-layer film (polyethylene(PE)/PE/TPU). The TPU film (thickness ≈ 40 μm) was then removed from the PE layers for the analyses. These different processes led to a small decrease in  $\overline{M}_w$  (3–4%).

### TPU Characterization

Differential scanning calorimetry (DSC) analysis was performed with a Mettler DSC 30 apparatus; samples of about 10 mg were taken from plates obtained by the compression molding of commercial pellets (170 °C, 5 min). To take off the water initially contained in the polyurethane, we kept the samples at 110 °C for 10 min before the first temperature scan. Two scans (10 °C/min) were then successively recorded with rapid intermediate cooling (50 °C/min). Both materials displayed exactly the same behavior: in the first scan [Fig. 4(a)], a glass transition was observed at a low temperature [58237, glass-transition temperature ( $T_g$ ) = -24 °C, and 58245,  $T_g$  = -37 °C] and could be associated with the soft POE-rich domains. At a higher temperature, between 100 and 200 °C, multiple endotherms, presumably related to the progressive disorganization of MDI–BDO hard domains, were detected. Depending on their length and terminal units, the melting of model MDI–BDO hard segments was shown to occur in this broad temperature range (12). This behavior thus reflected a partially phase-separated microstructure, but in any case, the melting enthalpy was low (~ 10 J/g, i.e., 3–3.5 kJ/equiv of urethane), whereas pure MDI/BDO hard segments of about the same length (three MDI units) showed a melting enthalpy  $\Delta H_m \approx 95$  J/g (i.e., 16–17 kJ/equiv of urethane (12)). This is consistent with the low  $x$  values evaluated by NMR (as discussed previously). In contrast, we could expect that after this first scan, followed by rapid cooling, the materials would be entirely amorphous. In the second scans [Fig. 4(b)], the observed  $T_g$  values were indeed higher (58237, +1 °C, and 58245, -19 °C); above  $T_g$ , sharp crystallization exotherms (67–71 °C) and corresponding melting endotherms (156–160 °C) of equal areas appeared and presumably reflected the phase separation of the hard domains.

**Table 1.** <sup>1</sup>H NMR Analysis of Unmodified Estane 58237 and Estane 58245 (DMSO-*d*<sub>6</sub>, 90 °C, 400 MHz)

Proton type <sup>a</sup>	δ (ppm)	Theoretical integration <sup>a</sup>	Peak integration (58237)	Peak integration (58245)	<i>x</i> (58237)	<i>n</i> (58237)	<i>x</i> (58245) <sup>d</sup>	<i>n</i> (58245)
a	1.72	4 <i>xα</i>	2.811	2.798	2.34 <sup>b</sup> / 2.38 <sup>c</sup>	21.34 <sup>b</sup> / 21.66 <sup>c</sup>	2.66	33.28
b	3.52 – 3.56	4( <i>n</i> – 2) <i>α</i>	23.263	b + b' =	2.23 <sup>b</sup> / 2.28 <sup>c</sup>		2.73	
b'	3.64	4 <i>α</i>	1.183	33.895				
c	3.79	2( <i>x</i> + 1) <i>α</i>	1.940	1.956	2.35 <sup>b</sup> / 2.41 <sup>c</sup>	2.79		
d	4.10	4 <i>xα</i>	2.816	2.814	2.30 <sup>b</sup> / 2.36 <sup>c</sup>	2.83		
d'	4.17 – 4.18	4 <i>α</i>	1.203	1.050	2.02 <sup>b</sup> / 2.07 <sup>c</sup>	2.29		
e	7.06	4( <i>x</i> + 1) <i>α</i>	4.031	3.980	Average value (rejecting <i>g</i> ): <i>x</i> = 2.34	Average value: 21.5	Average value (rejecting <i>g</i> ): <i>x</i> = 2.74	
f	7.34	4( <i>x</i> + 1) <i>α</i>	3.971	4.017				
g	9.17	2( <i>x</i> + 1) <i>α</i>	1.815	1.725				

<sup>a</sup> According to the structure proposed in Figure 2

<sup>b</sup> Using 4*α* = 1.203.

<sup>c</sup> Using 4*α* = 1.183.

<sup>d</sup> Using 4*α* = 1.050.

**Table 2.**  $^{13}\text{C}$  NMR Analysis of unmodified Estane 58237 and Estane 58245 (DMSO-*d*6, 25 °C, 100 MHz)

Carbon type <sup>a</sup>	$\delta$ (ppm)	Theoretical integration <sup>a</sup>	Peak integration (58237)	$x$ (58237)	$n$ (58237)
1	25.27	$2x\beta$	1.373	2.31 <sup>b</sup> / 2.51 <sup>c</sup>	22.45
2	63.39	$2\beta$	0.594		
3	63.67	$2x\beta$	1.211	2.04 <sup>b</sup> / 2.22 <sup>c</sup>	
4	68.71	$2\beta$	0.546		
5	69.81	$2(n - 2)\beta$	12.149		
6	118.74	$4(x + 1)\beta$	3.890	2.27 <sup>b</sup> / 2.56 <sup>c</sup>	
7	128.61	$4(x + 1)\beta$	4.026	2.39 <sup>b</sup> / 2.69 <sup>c</sup>	
8	135.41	$2(x + 1)\beta$	1.870	2.15 <sup>b</sup> / 2.42 <sup>c</sup>	
9	137.02	$2(x + 1)\beta$	1.990	2.35 <sup>b</sup> / 2.64 <sup>c</sup>	
10	153.47	$2\beta$	0.594		
11	153.60	$2x\beta$	1.526	2.57 <sup>b</sup> / 2.79 <sup>c</sup>	
12	$\approx 40$	$(x + 1)\beta$	Non detectable (DMSO)	Average value: $x = 2.42$	

<sup>a</sup> According to the structure proposed in Figure 2.

<sup>b</sup> Using  $2\beta = 0.594$ .

<sup>c</sup> Using  $2\beta = 0.546$ .

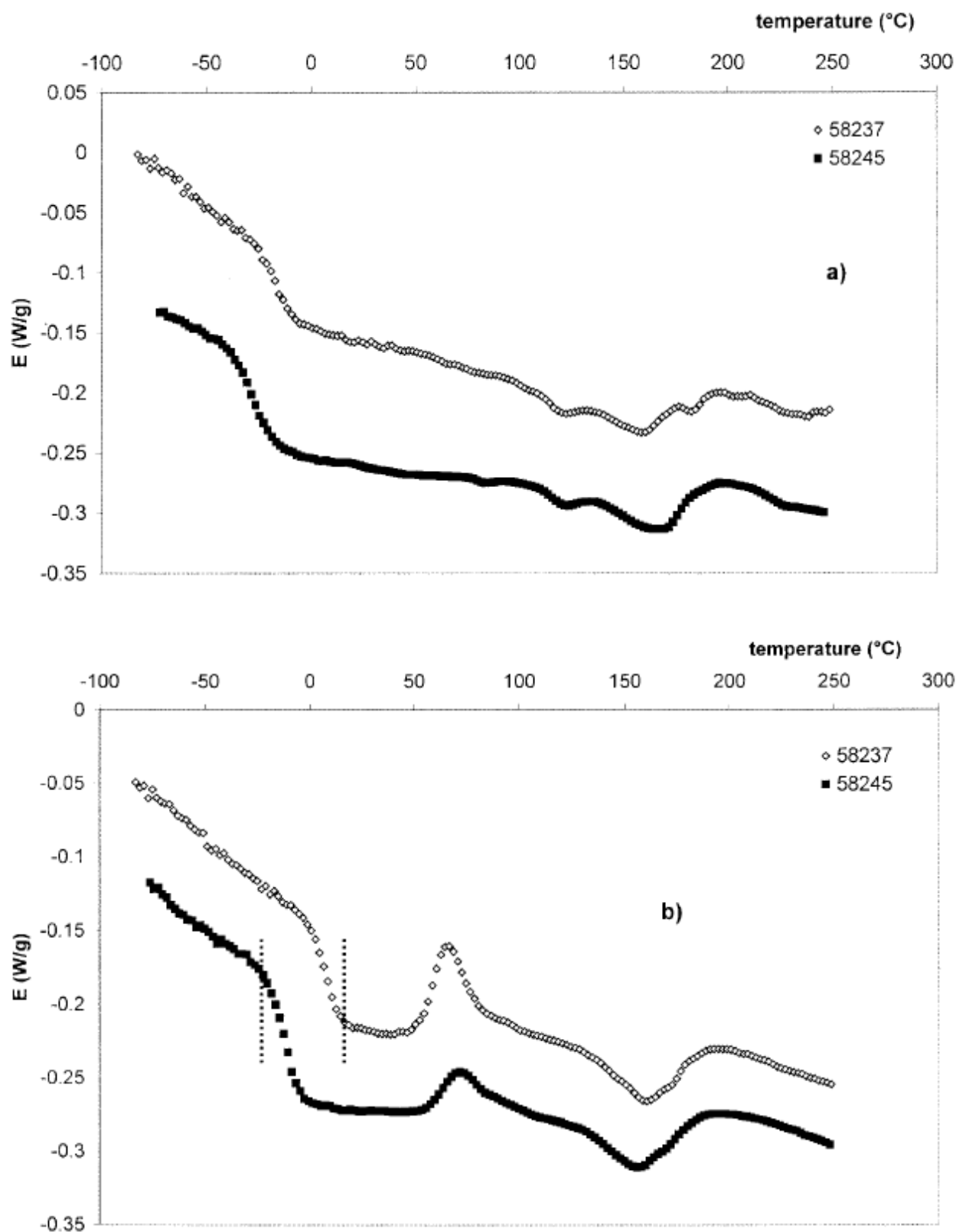


**Figure 4.** DSC thermograms of Estane 58237 and Estane 58245: (a) first scan and (b) second scan. The dotted lines indicate the calculated  $T_g$  values.

According to Fox's law,

$$T_g = \frac{w_1}{T_{g1}} + \frac{w_2}{T_{g2}}$$

where  $w_i$  is the weight fraction of pure  $i$  and  $T_{g_i}$  is the glass-transition temperature of pure  $i$ .  $T_g$  of the wholly amorphous one-phase material can be evaluated by the consideration of a mixture of a pure POE–MDI soft polyurethane and pure MDI–BDO hard segments; more precisely, the molar mass of the POE segments should also be taken into account. Recently, Vatalis and Kehayoglou (13) measured  $T_g = -47$  °C (226 K) for a POE1000–MDI polymer (model for Estane 58237); from all their data,  $T_g \approx -73$  °C (200 K) could also be expected for POE1500–MDI (the model for Estane 58245).  $T_g$  of pure MDI–BDO hard segments was found to be equal to 107 °C (380 K) (14). Using these results and the weight fractions deduced from NMR, we found  $T_g = +14$  °C (287 K) for Estane 58237 and  $T_g = -19$  °C (254 K) for Estane 58245 (i.e., a good correlation with the experimental results). Moreover, no crystallinity of the soft POE phase was ever detected.

Thus, two main conclusions can be drawn from this analysis: a higher mobility of the PU55 soft segment in comparison with PU48 and an extremely low crystallinity of the two TPUs.

The different processes used to prepare the films did not lead to an increased degree of crystallinity for the TPUs. The same DSC scans performed on compression-molded plates and solvent-cast, coextruded, and blown films led to exactly the same melting enthalpy of the hard segments (10 J/g), showing that these processes had no influence on the crystallinity degree of the material.

Furthermore, X-ray diffraction was performed on solvent-cast films with a Siemens D500 instrument equipped with a copper cathode and an Xray source ( $\lambda = 0.154$  nm). The spectra (Fig. 5), recorded at  $2\theta < 50^\circ$  with a step of  $0.02^\circ$ , do not show the presence of a crystalline phase.

Finally, we verified that no orientation effects were notably induced by the blowing–coextrusion process. The tensile properties were studied with an MTS 2/M apparatus for the films obtained by this method. The tensile stress and the elongation at break were determined at 22 °C on specimen equilibrated at 50% relative humidity at a strain rate equal to 200 mm/min. The mechanical properties were determined in the extrusion direction and in the transverse direction. The results are reported in Table 3, and they do not show any anisotropy of the samples.

Thus, from all these results, we can conclude that the differences in the TPU water transport properties are only related to the chemical compositions of the TPUs.

**Table 3.** PU55 Mechanical Properties: Tensile Stress ( $\sigma_R$ ) and Tensile Strain ( $\epsilon_R$ )

Film process TPU	Blowing extrusion Estane 58245 (PU55)	
Mechanical properties	Extrusion direction	Transverse direction
$\sigma_R$ (MPa)	45.3 ± 3.3	44.6 ± 1.9
$\epsilon_R$ (%)	1172 ± 72	1218 ± 47

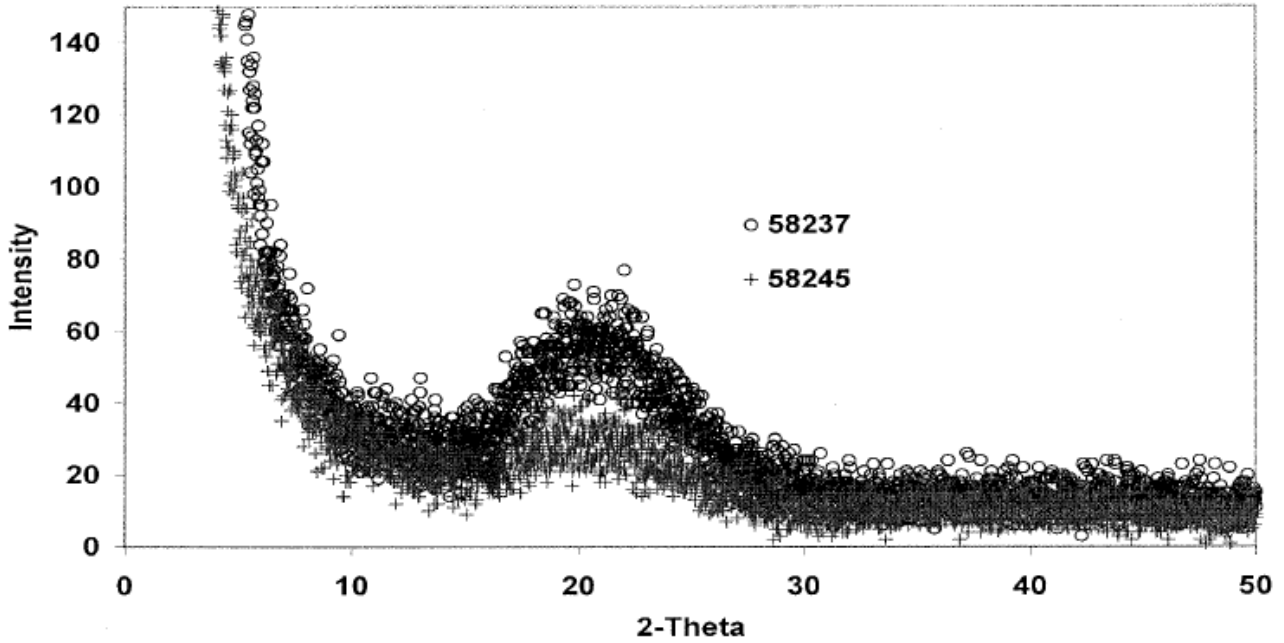


Figure 5. X-ray diffraction spectra of PU55 and PU48 films.

## Water Vapor Transport Properties

### Sorption Analysis

The samples (40 mg) were introduced into a Setaram B92 microbalance. The first step consisted of desorption *in vacuo* ( $2 \times 10^{-6}$  mbar) at a constant temperature ( $21 \pm 1$  °C) until a constant weight was obtained. This allowed us to determine the dry weight of the sample. The second step consisted of the establishment of a given partial pressure of water within the apparatus by means of an evaporator placed at a temperature  $T$ . The water vapor uptake ( $M_t$ ) was followed as a function of time until the equilibrium sorption ( $M$ ) was attained. Different experiments were carried out at different water partial pressures (changing  $T$  of the evaporator) to cover the entire range of  $a_w$ . The results obtained with the different studied polymers could be compared because  $M_t$  and  $M$  were expressed as the weight of the sorbed water vapor (g) per 100 g of the considered dry polymer. Two characteristics were studied from these experimental data: the kinetics of water sorption and the sorption isotherm.

*Kinetics of Water Sorption.* In the case of a Fickian mechanism, the diffusion of water is assumed to follow Fick's second law (15):

$$\frac{\partial C}{\partial t} = D \cdot \left( \frac{\partial^2 C}{\partial x^2} \right) \quad (1)$$

where  $D$  is the diffusion coefficient,  $t$  is the time,  $x$  is the position in the film, and  $C$  is the concentration of the sorbed molecules.

A simplified solution of this equation is obtained by the introduction of boundary conditions:

1. The upstream surface equilibrium is reached instantaneously.
2. The concentration of sorbed molecules is equal to 0 for  $t = 0$  at each point inside the specimen.
3. The downstream surface desorption is instantaneous.

Using the thickness of the film ( $e$ ), we obtain

$$\frac{M(t)}{M} = \left( 1 - \frac{8}{\pi^2} \cdot \sum_{n=0}^{\infty} \left[ \frac{1}{(2n+1)^2} \cdot \exp \left( \frac{-D \cdot \pi^2 \cdot (2n+1)^2 \cdot t}{e^2} \right) \right] \right) \quad (2)$$

For each partial pressure, the value of  $D$  can be computed by iterative calculations leading to the best fit of the experimental data by theoretical equation. It can also be calculated in different domains. A first value ( $D_1$ ) can be determined for  $Mt/M < 0.5$ ; eq 2 becomes

$$\frac{Mt}{M} = \frac{4}{e} \sqrt{\frac{Dt}{\pi}} \quad (3)$$

For  $Mt/M > 0.5$ , diffusion coefficient  $D_2$  can be obtained as follows:

$$\ln\left(1 - \frac{Mt}{M}\right) = \ln\left(\frac{8}{\pi^2}\right) - \frac{\pi^2 D_2 t}{e^2} \quad (4)$$

*Sorption Isotherm.* This represents  $M$  as a function of  $a_w$ . Its shape, indicative of the sorption mechanism, was analyzed with different models (discussed later). A mean solubility coefficient ( $S$ ;  $\text{cm}^3_{\text{STP}}/\text{cm}^3_{\text{polymer}} \text{cm}_{\text{Hg}}$ ) could be deduced from the mean slope of the isotherm.

The isotherm study was coupled with a calorimetric analysis. For each partial pressure increment, the thermal changes associated with the water uptake were recorded. The peak was integrated and corrected with energy values obtained under the same conditions with empty boats. The ratio of the obtained energy to the water uptake gave the interaction enthalpy ( $\text{kJ mol}^{-1}$ ). It was representative of the internal enthalpy change of one molecule from the gaseous state to the sorbed state.

### **Permeation Analysis**

The permeation cell consisted of two compartments separated by the studied membrane (sample area  $A = 20 \text{ cm}^2$ ,  $e = 40 \text{ }\mu\text{m}$ ). The cell was thermostated at  $21 \pm 1 \text{ }^\circ\text{C}$ . A preliminary high-vacuum desorption was realized in a permeameter. This first step allowed us to desorb the sample and also to ensure that the static vacuum pressure changes in the downstream compartment were smaller than the pressure changes due to the water vapor diffusion.

Water vapor pressure  $P_1$  was then established by means of an evaporator in the upstream compartment, and it was kept constant. Pressure  $P_2$  in the downstream compartment with downstream volume  $V_2$  was measured as a function of time. Under our experimental conditions, as the water molecules diffused through the film, the downstream pressure increased progressively to attain the value of upstream pressure  $P_1$ . Thus, the pressure gradient between the upstream and downstream faces of the membrane varied during a given experiment: it decreased as a function of time.

The permeability coefficient ( $P$ ), expressed in barrer units ( $1 \text{ barrer} = 10^{-10} \text{ cm}_{\text{STP}} \text{ cm cm}^{-2} \text{ s}^{-1} \text{ cm}_{\text{Hg}}^{-1}$ ), was calculated by two methods. The first one consisted of determining the slope of the curve representative of  $J$  through the membrane as a function of the pressure gradient:

$$P = \frac{Je}{(P_1 - P_2)} \quad (5)$$

$$J = \frac{d(P_2 V_2)}{76 A dt} \quad (6)$$

For the second method,  $J$  was expressed with eqs 5 and 6, and the following first-order differential equation was obtained:

$$\frac{dP_2}{dt} + \frac{76PA}{eV_2} P_2 = \frac{76PA}{eV_2} P_1 \quad (7)$$

The variation of  $P_2$  could then be expressed as a function of  $P_1$  and  $t$ :

$$P_2 = P_1 \left[ 1 - \exp\left(\frac{76PA}{eV_2}\right) t \right] \quad (8)$$

$P$  could be obtained from the slope of the curve  $\ln[P_1/(P_1 - P_2)]$  versus time:

$$P = \frac{eV_2}{76A} \frac{d\left(\ln\frac{P_1}{P_1 - P_2}\right)}{dt} \quad (9)$$

where  $A$  is the membrane area.

## RESULTS AND DISCUSSION

### Water Vapor Sorption

The water sorption was studied at 21 °C for different values of  $a_w$ .

For each partial pressure, sorption data were plotted versus the square root of time, and the ratio  $M_t/M$  was plotted as a function of time. In the first part, the results obtained for the PU55 cast film presented in Figures 6 and 7 are discussed. The second part concerns the influence of the film process and the TPU composition.

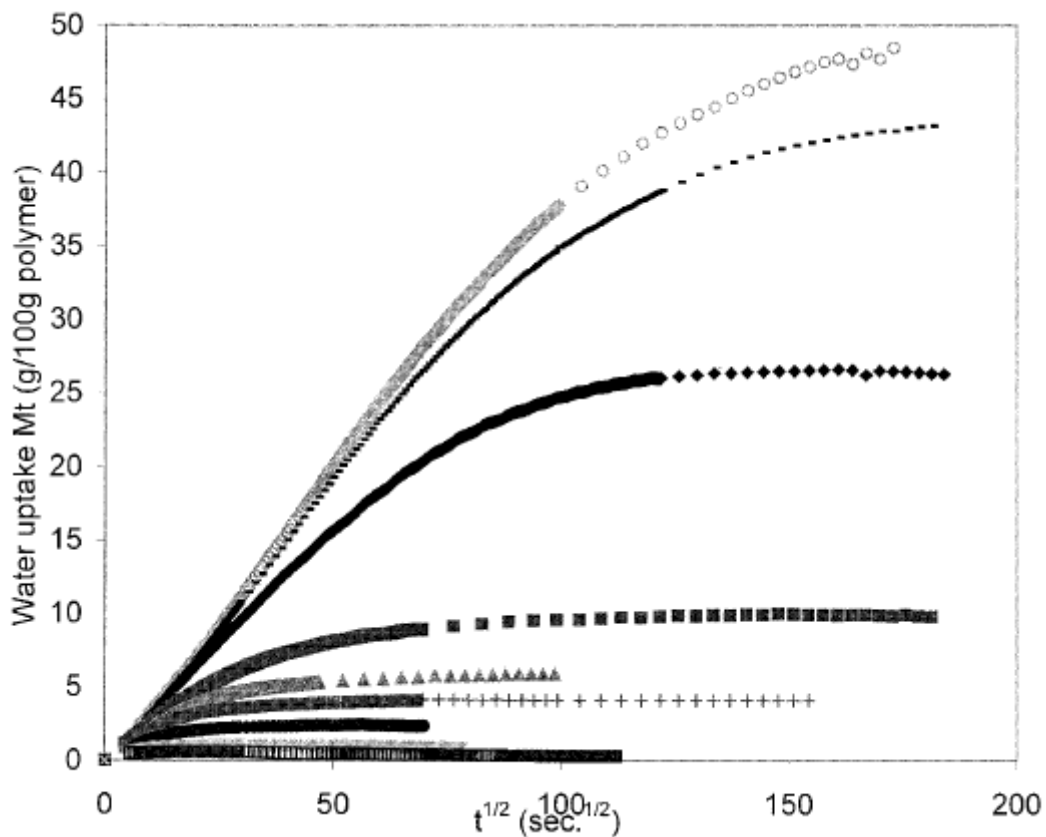


**Figure 6.** Variation of  $M_t$  of PU55 as a function of  $t^{1/2}$  for different values of  $a_w$ : (□)  $a_w = 0.2$ , (×)  $a_w = 0.3$ , (●)  $a_w = 0.48$ , (+)  $a_w = 0.58$ , (▲)  $a_w = 0.7$ , (■)  $a_w = 0.8$ , (◆)  $a_w = 0.91$ , (—)  $a_w = 0.94$ , and (○)  $a_w = 0.99$ .

Figure 6 clearly shows that  $M$  increases as  $a_w$  increases. The kinetics are fast. Indeed, for  $a_w < 0.4$ , the sorption equilibrium is obtained instantaneously for  $e = 40 \mu\text{m}$ , and it is not possible to determine the initial slope of the curve representative of  $M_t$  as a function of  $t^{1/2}$ . For a higher value of  $a_w$ , the sorption rates decrease. This trend is confirmed by the increase of the time at half-sorption ( $t^{1/2}$ ) corresponding to  $M_t/M = 0.5$  (Fig. 7). The

linear shape of the water sorption curves, as a function of the square root of time up to about 70% of  $M$  indicates that sorption is controlled by a Fickian mechanism (Fig. 6). The  $D$  values were thus calculated according to eqs 3 and 4 according to the range of  $a_w$ . The results obtained for the PU55 cast film and coextruded film are reported in Table 4.

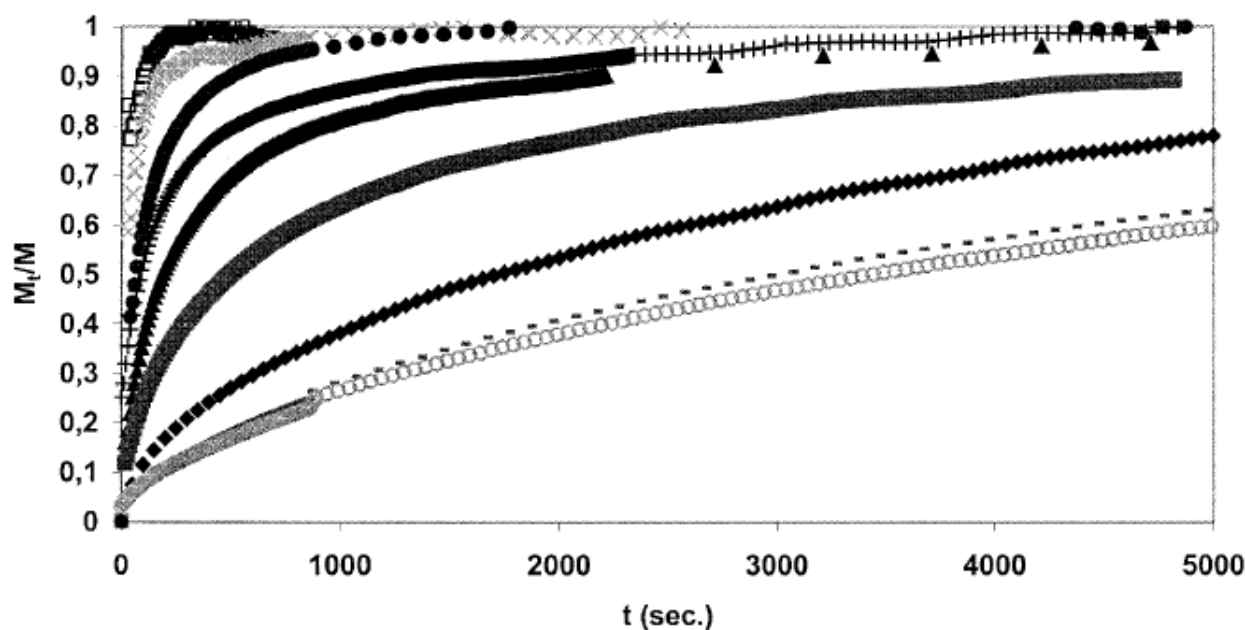


**Figure 7.** Evolution of  $M_t/M$  as a function of time for different values of  $a_w$  for PU55: ( $\square$ )  $a_w = 0.2$ , ( $\times$ )  $a_w = 0.3$ , ( $\bullet$ )  $a_w = 0.48$ , ( $+$ )  $a_w = 0.58$ , ( $\blacktriangle$ )  $a_w = 0.7$ , ( $\blacksquare$ )  $a_w = 0.8$ , ( $\blacklozenge$ )  $a_w = 0.91$ , ( $-$ )  $a_w = 0.94$ , and ( $\circ$ )  $a_w = 0.99$ .

For  $a_w < 0.5$ ,  $D$  values of  $1\text{--}2 \times 10^{-8} \text{ cm}^2 \text{ s}^{-1}$  have been obtained. For a higher value of  $a_w$ , a decrease in  $D$  as a function of the partial pressure can be noticed, and near saturation, the  $D$  values are around  $2 \times 10^{-10} \text{ cm}^2 \text{ s}^{-1}$ , thus divided by a factor 100 in comparison with the values determined at low values of  $a_w$ . For a given sorption experiment,  $D_2$  values are lower than  $D_1$  values. From all these results, it can be concluded that the  $D$  values are concentration-dependent.

No great differences are observed for the  $D$  values as a function of the process used to prepare the films (Table 4).

However, the modification of the TPU composition leads to a significant variation in the water sorption kinetics. Indeed, lower  $D$  values are measured for PU48 (Fig. 8). They are almost divided by a factor of 5 in comparison with PU55. As for PU55, small variations of  $D$  can be observed for  $a_w = 0\text{--}0.45$ . For higher values of  $a_w$ ,  $D$  decreases as  $a_w$  increases. This behavior has already been observed in the literature for some polymers (11,16–20), and it is generally related to a water clustering mechanism. In this case, the water–water interactions become the predominant phenomenon leading to the formation of larger entities. As a result, a decrease in the apparent diffusion is observed. The analysis of the sorption isotherm can confirm this phenomenon and bring further information.

### Sorption Isotherm

The water sorption isotherms with respect to the two TPUs can be described by an exponential curve, as shown in Figure 9(a). This type of isotherm is also called a type III isotherm in reference to the BET classification (21). For  $a_w = 0\text{--}0.45$ ,  $M$  is low and increases quite linearly as  $a_w$  increases. For higher values of  $a_w$ , the increase in  $M$  becomes very important. Near saturation ( $a_w \approx 1$ ),  $M$  is about

50 g/100 g of dry polymer for PU55. As for the  $D$  values, no significant differences have been noticed as a function of the process used to prepare the films (casting or blowing coextrusion). However, an influence of the TPU composition can be observed. Indeed,  $M$  is lower for PU48 than for PU55. Nevertheless, these uptakes still remain important for  $a_w > 0.8$ . The importance of the soft block structure for the water sorption ability has already been mentioned in the literature. Schneider et al. (22) showed that the use of POE as a soft segment led to higher water sorption than other polyethers [e.g., poly(tetramethylene oxide) or poly(propylene oxide)] or polyester [(poly(butylene adipate)]. For MDI/POE polyurethanes, Petrick et al. (6) underlined an exponential increase in the liquid water sorption as a function of the polymer soft block content. For polyurethanes based on mixed soft blocks, either linear or exponential variations of the liquid water uptake as a function of the POE content have been noticed (5,23). The predominant role of POE segments in the liquid water uptake is thus underlined in the literature.

**Table 4.**  $D_1$  and  $D_2$  Determined at Different Values of  $a_w$  for PU55 Films Obtained by Different Processes

Film process				
	Casting		Blowing coextrusion	
$a_w$	$D_1$ ( $10^{-9} \text{ cm}^2 \text{ s}^{-1}$ )	$D_2$ ( $10^{-9} \text{ cm}^2 \text{ s}^{-1}$ )	$D_1$ ( $10^{-9} \text{ cm}^2 \text{ s}^{-1}$ )	$D_2$ ( $10^{-9} \text{ cm}^2 \text{ s}^{-1}$ )
0.2	<sup>a</sup>	24.6	<sup>a</sup>	20.3
0.3	<sup>b</sup>	<sup>b</sup>	<sup>a</sup>	15.8
0.4	<sup>a</sup>	12.4	<sup>b</sup>	<sup>b</sup>
0.48	<sup>b</sup>	<sup>b</sup>	12.1	5.6
0.58	7.9	2.6	8	2.7
0.7	4.7	2.0	4.3	1.9
0.8	1.4	0.9	1.6	0.85
0.91	0.5	0.4	0.46	0.4
0.99	<sup>b</sup>	<sup>b</sup>	0.23	0.2

<sup>a</sup>  $D$  values cannot be calculated.

<sup>b</sup>  $D$  values have not been determined.

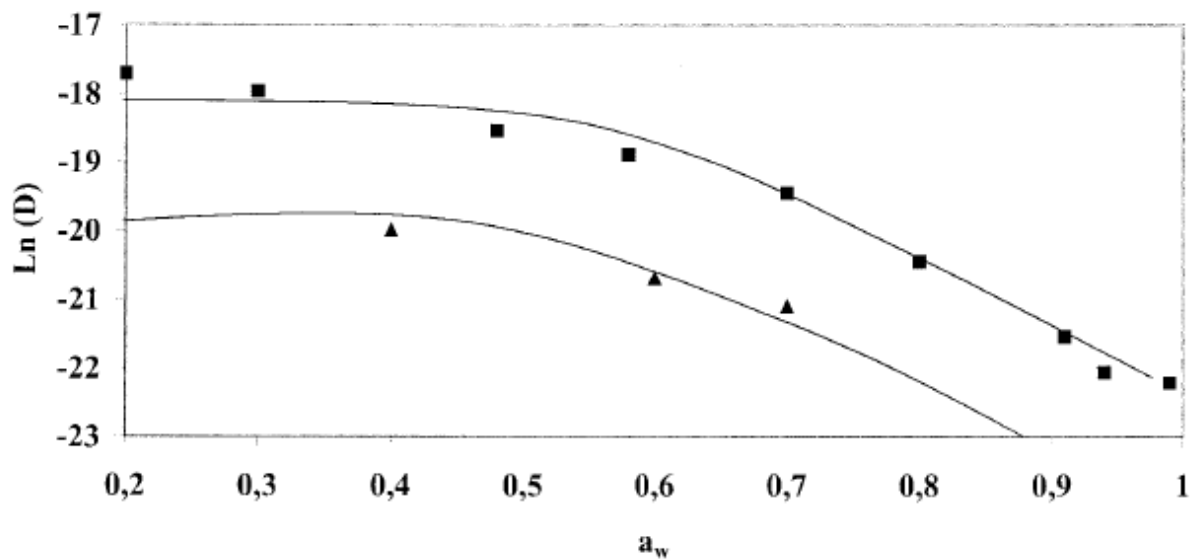


**Figure 8.** Evolution of  $D_2$  as a function of  $a_w$  for (▲) PU48 cast films and (■) PU55.

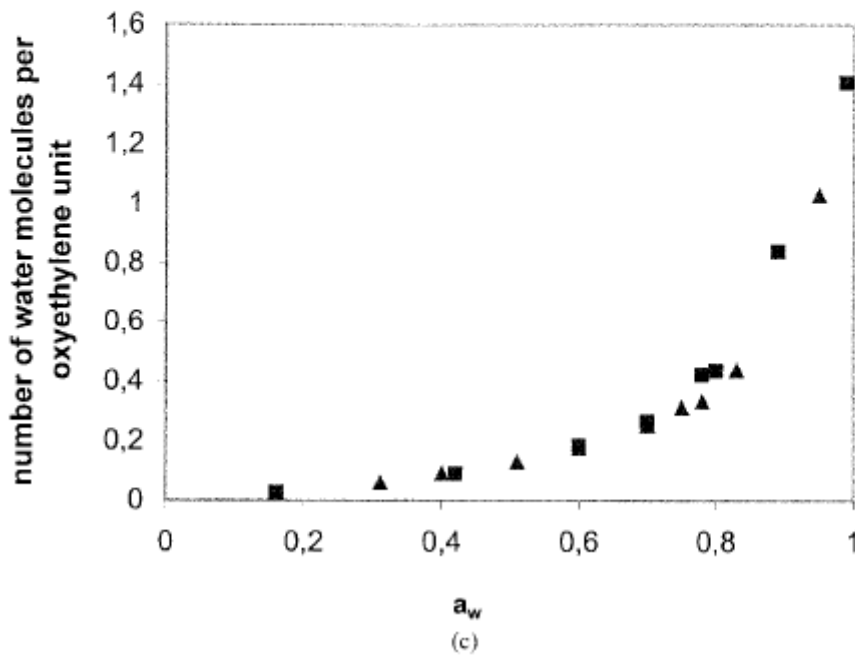
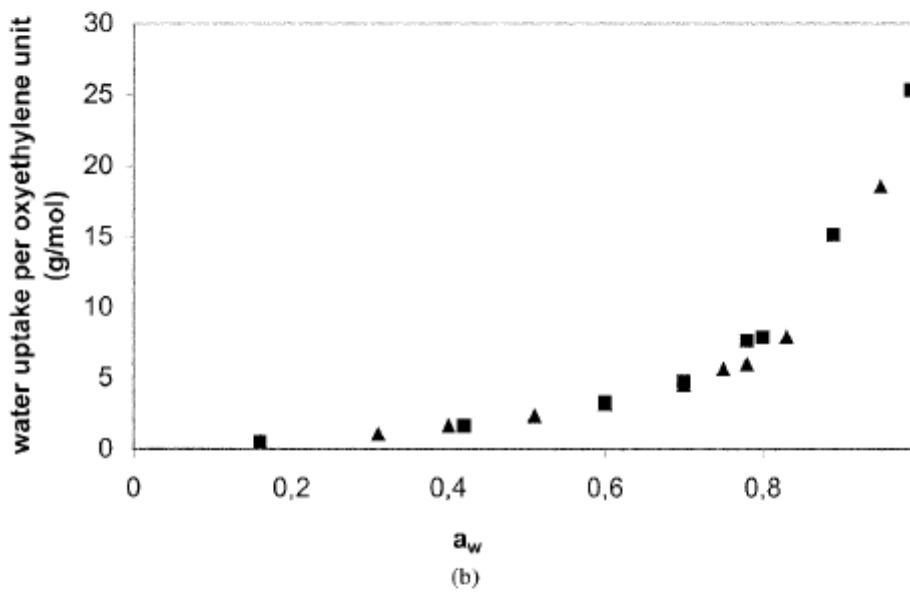
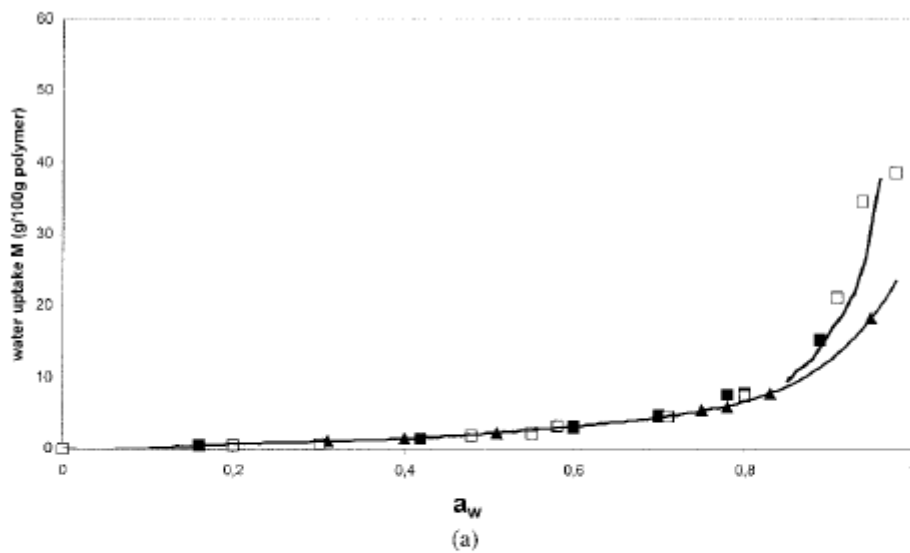


**Figure 9.** (a) Water sorption isotherms, (b) water uptake per OE unit at equilibrium as a function of  $a_w$ , and (c) number of water molecules sorbed per OE unit at equilibrium as a function of  $a_w$  for (▲) a PU48 cast film, (■) a PU55 cast film, and (□) a PU55 coextruded film.

Nevertheless, very few results concern water vapor uptake. As the major differences between the two polyurethanes studied consist of the length of the soft segment and, as a result, the POE content, the sorption data have been represented for the two TPUs as the amount of water vapor sorbed per oxyethylene (OE) unit [Fig. 9(b,c)]. A lonely isotherm has been obtained for the two TPUs, confirming that in these systems, the POE hydrophilic soft segments plays the major role in the sorption mechanism.

Complementary information can be obtained by the analysis of the differential molar enthalpy of interaction. The enthalpy profiles are similar for the two TPUs and are quite smooth. In particular, the enthalpy values at low partial pressures are not very high in the absolute value ( $\approx -50$  kJ/mol), excluding strong interactions between the first water molecules sorbed and the TPU chains. This result is consistent with the quite linear shape of the isotherm at a low value of  $a_w$  and with the participation of POE soft segments in the sorption mechanism because they are capable of much weaker interactions with water than ester groups or urethane groups, for example. At a high value of  $a_w$ , the enthalpy values become similar to the liquefaction water enthalpy ( $\approx -40$  kJ/mol).

In the following part of the study, different models have been used to obtain more details on the sorption mechanism, particularly with respect to the important increase in the water uptakes noticed at high activities. Three approaches have been investigated: the conventional solution theory (e.g., the Flory–Huggins theory) (24); the Brown model (25), which combines the Flory–Huggins approach and the Zimm–Lundberg cluster theory (26); and the Guggenheim–Anderson–de Boer model (27–29), which has already been used to describe BET type II and type III isotherms (30,31). The curve-fitting efficiency is estimated from the classical coefficient  $R^2$  and from the residual sum of squares (RSS) defined by

$$RSS = \sum (y_{exp} - y_{calc})^2 \quad (10)$$

where  $y_{exp}$  and  $y_{calc}$  are the reported experimental and corresponding calculated values, respectively. The RSS values obtained from the regression of a given set of experimental data by different models allow a direct and statistically significant comparison of the results obtained by the different fittings. As no influence of the process has been observed on the sorption isotherms, this analysis has been developed for PU55 and PU48 cast films.

The Flory–Huggins (24) equation relates the volume fraction of the solvent ( $\phi_1$ ) to  $a_w$ :

$$\ln a_w = \ln \phi_1 + (1 - \phi_1) + \chi(1 - \phi_1)^2 \quad (11)$$

The isotherm can be predicted if the polymer–solvent interaction parameter ( $\chi$ ) is known.  $\chi$  is often assumed to be constant, and in that case, it is either calculated through the solubility parameter approach or deduced from the swelling of the polymer in the pure solvent. For some systems, it has been shown that  $\chi$  can change significantly as a function of the polymer volume fraction. In this last case, a variation law based on three adjustable parameters was proposed by Koningsveld and Kleinjens (32):

$$\chi = \alpha + \frac{\beta(1-\omega)}{(1-\omega\phi_p)^2} \quad (12)$$

where  $\alpha$  is an empirical correction term and  $\beta$  and  $\omega$  are two parameters related to the mixing enthalpy and the coordination number of the system, respectively. The sorption isotherm of PU48 and PU55 cannot be described with a constant value of  $\chi$ . However, it can be correctly predicted by the coupling of the Koningsveld–Kleinjens approach to the Flory–Huggins equation. For activities ranging from 0.16 to 0.83,  $\chi$  values decrease from 2.13 to 0.98 and from 2.24 to 1.47 for PU55 and PU48, respectively. The values of the three adjustable parameters, allowing an adequate description of  $\chi$  variation and, consequently, an accurate description of the sorption isotherm, as shown in Figure 10(a) for PU55, are presented in Table 5. We can notice that  $\alpha$  and  $\omega$  decrease from PU48 to PU55 when the swelling capacity of the polymer increases. Favre

et al. (33), considering the swelling power of different liquids with respect to the same polymer (polydimethylsiloxane) (PDMS), observed the same trend. Nevertheless, any quantitative interpretation can be deduced from these gradations because of the empirical significance of the adjustable parameters. The main conclusion drawn from this analysis is that water cannot be considered a good solvent with respect to both considered TPUs.

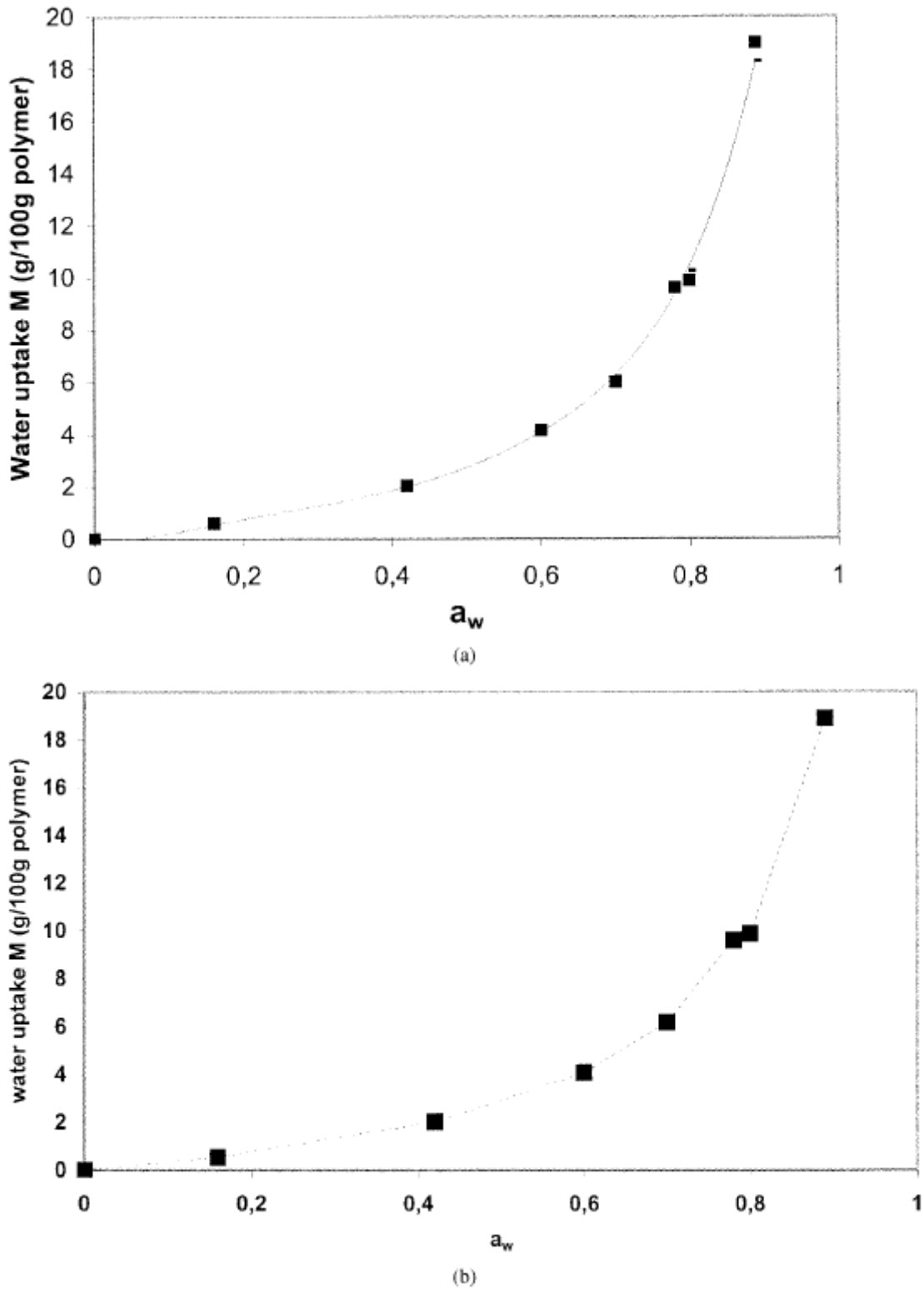


**Figure 10.** Comparison of (-) different models and (■) the experimental water sorption isotherm of PU55: (a) the combined Flory–Huggins and Koningsveld–Kleinjens approach and (b) the GAB model.

To better analyze the sorption data at high activities, we used the Brown method (25). It combines the previously mentioned Flory–Huggins solution theory with the Zimm–Lundberg cluster theory. This theory has already been used to study the sorption of water molecules by poly(ethylene adipate)/MDI/BDO polyurethanes (34):

$$\frac{1}{\varphi_1} = \frac{k_1}{a_w} - k_2 \quad (13)$$

where  $\varphi_1$  is the volume of water sorbed at the sorption equilibrium ratioed to the dry polymer volume and  $k_1$  and  $k_2$  are two adjustable parameters. The value of  $k_2$  determines the type of isotherm. For  $k_2 = 0$ , a linear variation of  $\varphi_1$  as a function of  $a_w$  is observed, and a Henry's law sorption is obtained. Negative  $k_2$  values describe Langmuir or dual-mode sorption isotherms. Positive  $k_2$  values correspond to BET type III isotherms. In this last case, the amount of water sorbed is considered the sum of the water content corresponding to random mixing and the water content involved in an association or clustering phenomenon. Combining eq 11 with the Lundberg–Zimm cluster theory leads to different parameters from  $k_1$  and  $k_2$ , notably the average number of water molecules in a cluster ( $N_c$ ). The cluster integral ( $G_{11}$ ) was defined by Zimm and Lundberg (26) as follows:

$$\frac{G_{11}}{v_1} = -(1 - \varphi_1) \left[ \frac{\partial \left( \frac{a_w}{\varphi_1} \right)}{\partial a_w} \right]_{P,T} - 1 \quad (14)$$

where  $v_1$ ,  $\varphi_1$ , and  $a_w$  are the molecular volume, volume fraction, and activity of component 1, respectively.

The average number of solvent molecules in a cluster is defined as follows:

$$N_c = \varphi_1 \frac{G_{11}}{v_1} + 1 \quad (15)$$

For an ideal solution, there is no clustering, and  $N_c$  is equal to 1.

Combining eqs 13–15 gives an expression of  $N_c$  as a function of  $k_2$ :

$$N_c = 1 + k_2 \varphi_1 - k_2 \varphi_1^2 \quad (16)$$

$k_1$  and  $k_2$  values have been determined for PU55 and PU48 cast films by a plot of  $1/\varphi_1$  as a function of the inverse of  $a_w$  (Table 5), and  $N_c$  values have been calculated according to eq 16. Figure 11 presents the evolution of  $N_c$  as a function of  $a_w$ .  $N_c$  increases progressively to attain a value equal to 2 at  $a_w = 0.6$ . For higher values of  $a_w$ , the increase in  $N_c$  becomes more important. Furthermore,  $N_c$  values are slightly higher for PU55.

The results obtained by the Brown method were compared with those determined by the Guggenheim–Anderson–De Boer approach for one TPU: PU55.

The GAB equation has been widely used to study water sorption in foods and natural and synthetic polymers (30,31), and according to the literature, it can describe type II and type III BET isotherms. The equation is based on three adjustable parameters:

$$M = \frac{a_{GAB} c_{P,GAB} k a_w}{(1 - k a_w)} * \frac{1}{1 + (c_{P,GAB} - 1) k a_w} \quad (17)$$

where  $c_{P,GAB}$  is the Guggenheim constant,  $a_{GAB}$  is the monolayer water content, and  $k$  is the factor correcting properties of the multilayer molecules with respect to the bulk liquid. In the GAB model,  $k$  is less than 1 as the heat of adsorption is lower than the corresponding heat of condensation.

**Table 5.** Parameters of the Different Models Used to Describe the TPU Sorption Isotherm

Model	Parameters	PU48	PU55
Combined Flory–Huggins and Koningsveld–Kleinjens	$\alpha$	1.258	0.717
	$\beta$	0.069	0.175
	$\omega$	0.944	0.894
	RSS	0.016	0.02
Brown	$k_1$	34.897	31.362
	$k_2$	29.29	28.557
	$R^2$	0.9993	0.9993
Guggenheim–Anderson–De Boer	$C_{P,GAB}$	Not determined	1.113
	$a_{GAB}$	Not determined	0.0274
	$k$	Not determined	0.98
	RSS		0.000037

<sup>a</sup>  $R^2$  and RSS are correlation coefficients.

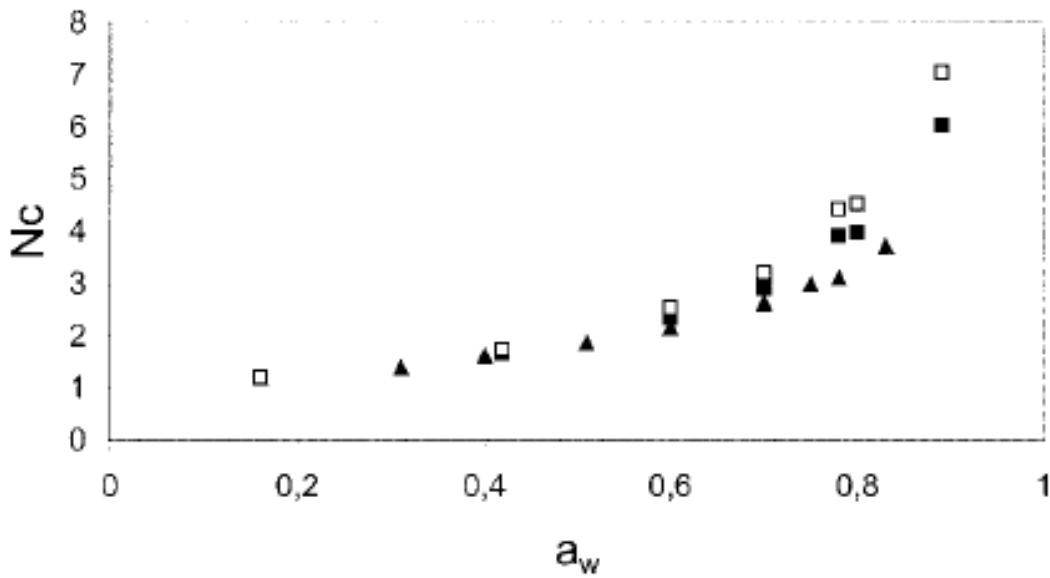


**Figure 11.** Evolution of  $N_c$  as a function of the partial pressure according to the Brown approach for ( $\blacktriangle$ ) PU48 and ( $\blacksquare$ ) PU55 and according to the Zhang and GAB approaches for ( $\square$ ) PU55.

The GAB model allows the accurate description of the water vapor sorption properties of PU55 over the entire range of partial pressures [Fig. 10(b)]. The GAB parameters are reported in Table 5, and we can notice that  $a_{GAB}$  is small and  $k$  is near to 1.  $N_c$  values have been deduced from the GAB model parameters with the Zhang equation:

$$N_c = -(1 - \varphi_1) \times \left[ \frac{\varphi_1}{a_{GAB} c_{P,GAB}} (-2c_{P,GAB} k a_w + 2k a_w + c_{P,GAB} - 2) - 1 \right] \quad (18)$$

The results are reported in Figure 11. A good agreement is observed between the results obtained by this model and the Brown approach.

## Water Vapor Permeation

The water permeation was studied for the entire range of  $a_w$ .

For  $a_w < 0.6$ , the variation of  $J$  as a function of the pressure gradient applied to the membrane is linear [Fig. 12(a)]. The evolution of  $\ln[P_1/(P_1 - P_2)]$  versus time shows a transitory state followed by a steady state for which a single slope can be determined [Fig. 12(b)]. Thus, a single  $P$  value can be calculated for each experiment. For PU55,  $P = 700$  barrer has been determined at a relative pressure equal to 0.4.

For  $a_w > 0.6$ , the variation of  $J$  as a function of the pressure gradient applied to the membrane during the experiments is no more linear [Fig. 13(a)], and different slopes can be determined from the curve of  $\ln[P_1/(P_1 - P_2)]$  versus time [Fig. 13(b)]. As a result, for a given experiment, a single  $P$  value cannot be calculated. Nevertheless, discrete values of  $P$  have been determined at 25 and 80% of the water transfer, and they are reported in Table 6 for the two polyurethanes at different activities.

**Table 6.** Water Permeability Coefficients of PU48 and PU55 at Different Values of  $a_w$

	$a_w$	0.4	0.6	0.7	0.8	0.9	0.99
Estane 58237	$P_{25\%}$ (barrer)	500	650	1,600	6,000	42,100	101,400
	$P_{80\%}$ (barrer)	500	700	4,000	15,900	136,900	243,300
Estane 58245	$P_{25\%}$ (barrer)	700	1,300	14,900	19,900	70,200	175,500
	$P_{80\%}$ (barrer)	700	1,400	69,600	74,200	175,500	509,000

<sup>a</sup> $P_{25\%}$  and  $P_{80\%}$  represent the water flux at 25 and 80% of the water vapor transfer, respectively.

Some tendencies can be drawn from these values. For  $a_w = 0-0.6$ , the  $P$  values of both TPUs do not depend on the water-transfer percentage, and their values are low. At higher values of  $a_w$ , the permeability increases as  $a_w$  increases, and for a given experiment, different values have to be considered. It can at last be observed that PU48 is less permeable to water vapor than PU55, especially at a high  $a_w$  value.

## DISCUSSION

From all the sorption and permeation results, a sorption mechanism can be proposed, and its implication in the evolution of  $J$  as a function of  $a_w$  can be established.

Thus, at low values of  $a_w$ , the water is distributed through the polymer mainly in the vicinity of the POE soft segments. The evolution of  $M$  as a function of  $a_w$  is linear, and the solubility can be determined by the slope of the isotherm. The solubility is small, and it stays quite constant around a value of  $25 \text{ cm}^3/\text{cm}^3 \text{ cmHg}$ . In this domain, the sorption mechanism is Fickian, and the interaction involved between the sorbed water molecules and the soft chains are not strong, as underlined by the calorimetric analysis. Partly because of the rubbery state of the polymer at  $21^\circ\text{C}$ , the water diffusion is fast.

At high water partial pressures, the water molecule association phenomenon occurs. A positive deviation from Henry's law is observed, the solubility greatly increases, and the apparent  $D$  value decreases. In this domain,  $N_c$  has been determined with a Brown analysis, and the results are in good agreement with those calculated from the GAB parameters. The clustering phenomenon does not occur on each OE unit because the number of water molecules sorbed per OE unit [Fig. 9(c)] does not correspond to the  $N_c$  values. It is lower.

No influence of the process used to realize the films has been noticed on the mechanical properties nor on the water sorption mechanism. It can be concluded that no orientation effect is induced by the blowing-coextrusion method.

The TPU composition has no influence on the sorption mechanism, but it has an influence on the level of both the water solubility and diffusion. Increasing the POE soft segment length leads to increased mobility of the TPU chains, as shown by the decrease in  $T_g$ , and to an increased water diffusion rate. The water uptake increases in proportion to the OE content in the polymer.

The differences in the sorption behaviors as a function of the composition and as a function of the  $a_w$  range imply some consequences on the permeation properties. Indeed, for  $a_w < 0.6$ , we have underlined a Henry-type sorption with a quite constant  $D$  value and a quite linear increase of the water uptake as a function of  $a_w$  and, therefore, a constant solubility parameter. As a result, the water permeability is constant. Despite the high diffusion rate,  $P$  is small, showing the importance of the solubility parameter. Furthermore, as low differences have been observed in the solubility of PU48 and PU55, the permeability values measured for the two TPUs are quite similar.

For higher values of  $a_w$ , a positive deviation from Henry's law has been noticed in the sorption study. The solubility depends on the water vapor pressure applied to the sample, and it increases with this parameter.  $D$  is no longer constant but is concentration-dependent. As a result, the water flux does not remain constant when the pressure gradient varies during the experiment. It depends on the mean water pressure applied to the membrane and increases as this one increases because of the major effect, in this case also, of the solubility parameter. As the solubility is higher for PU55 than for PU48, higher permeability values are obtained.

Thus, the breathable character of the membranes depends on the mean water pressure. It is constant and low when the mean water pressure is less than 1 cm<sub>Hg</sub>; for higher values, it increases. This evolution is mainly due to a solubility effect and not to a diffusion effect. As a result, PU55 has the most interesting properties.

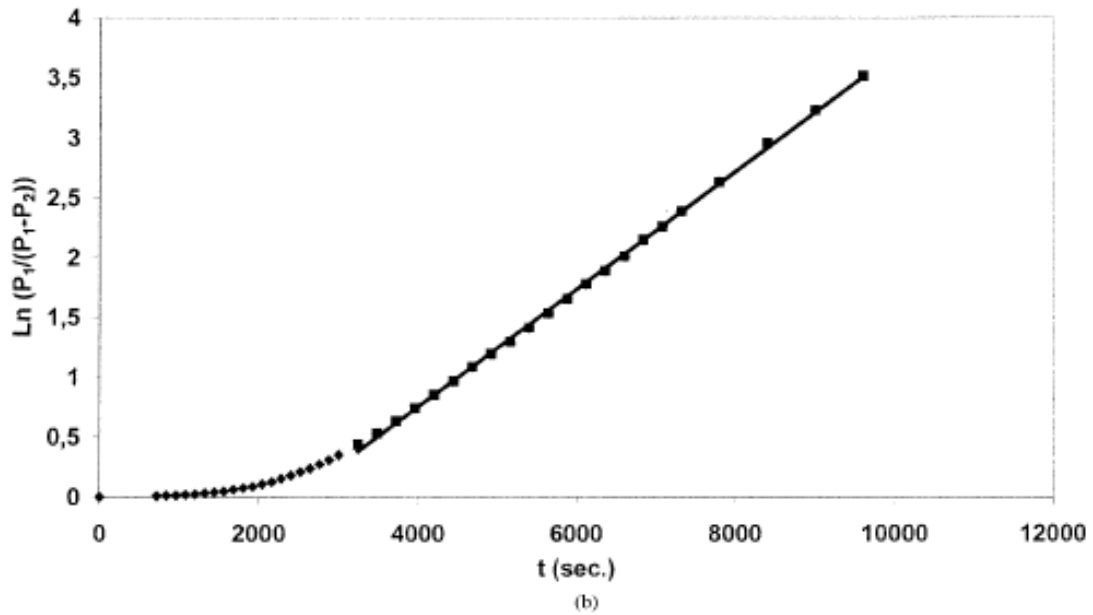
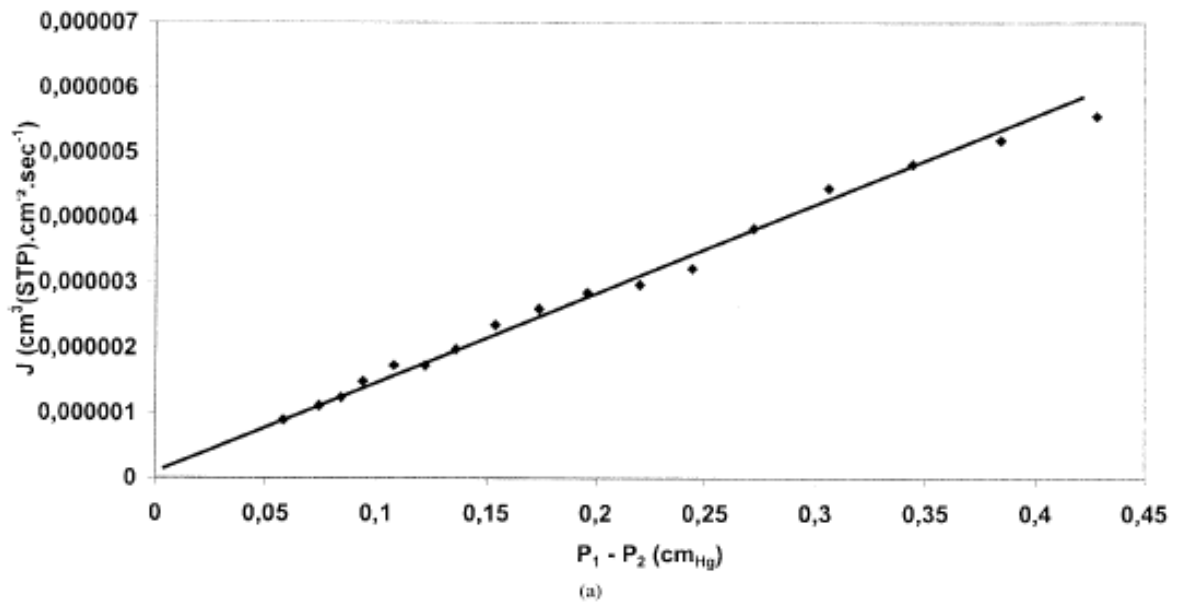
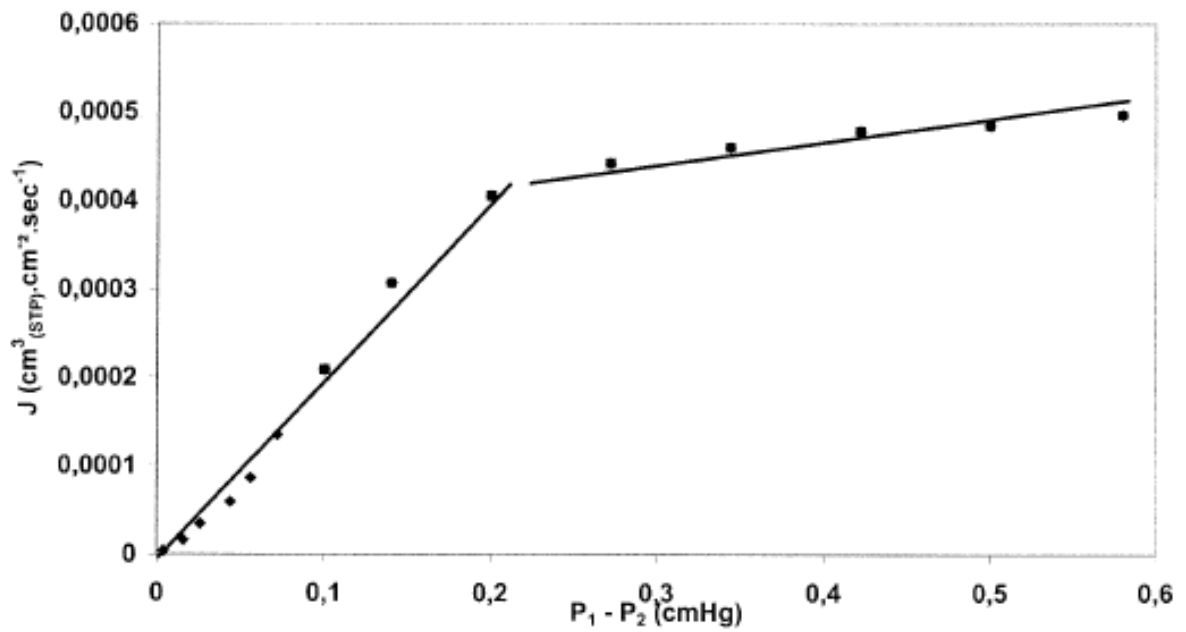
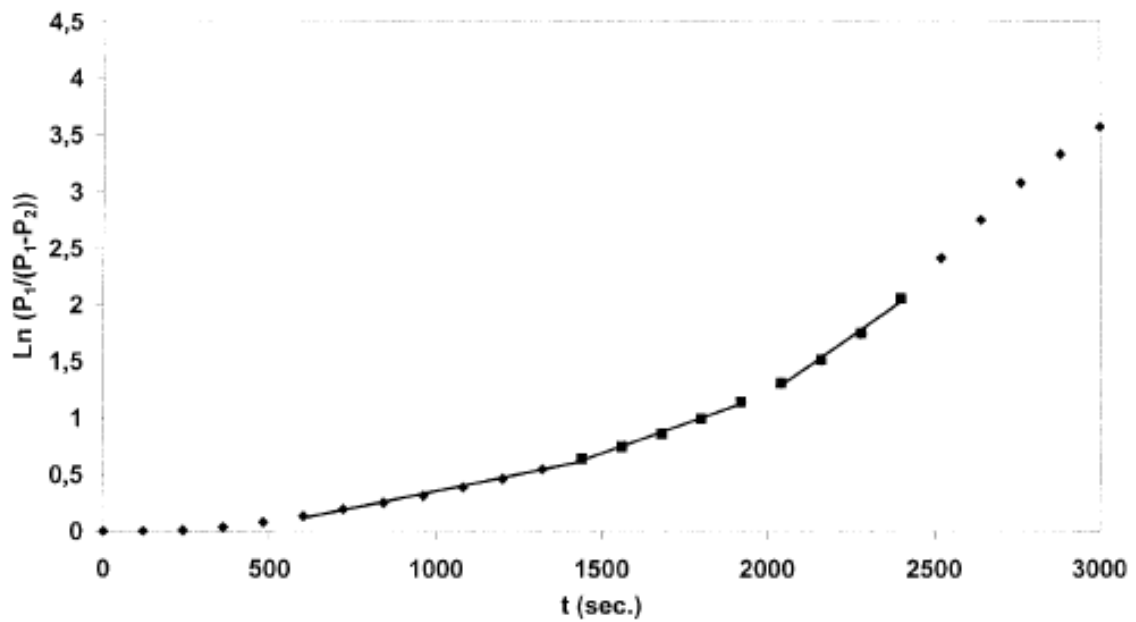


**Figure 12.** (a) Evolution of  $J$  as a function of the gradient pressure applied to the PU55 membrane for an experiment made at  $P/P_0 = 0.4$  and (b) evolution of  $\ln[P_1/(P_1 - P_2)]$  as a function of time for an experiment made at  $P/P_0 = 0.4$  for the PU55 film.



(a)



(b)

**Figure 13.** (a) Evolution of  $J$  as a function of the gradient pressure applied to the PU55 membrane for an experiment made at  $P/P_0 = 0.8$  and (b) evolution of  $\ln[P_1/(P_1 - P_2)]$  as a function of time for an experiment made at  $P/P_0 = 0.8$  for the PU55 film.

## CONCLUSIONS

Water sorption in Estane 58237 and Estane 58245 TPU films is governed by a Fickian mechanism. For partial pressures less than 0.4, the amount of sorbed water is mainly due to random mixing, whereas at higher relative pressures, an additional contribution due to water clustering is observed. In this last domain, a decrease in  $D$  is observed. Different models allow the accurate description of the sorption isotherm and also the determination of  $N_c$ . At  $a_w = 0.6$ , each cluster is composed of the association of two water molecules, and at higher values of  $a_w$ , this phenomenon predominates and the cluster mean size increases. As for water sorption, two domains are distinguished for water permeation. At relative pressures less than 0.6, the  $P$  values are low and easy to determine. For higher relative humidities, the water transport mechanism becomes more complex, and variations of  $P$  as a function of the pressure gradient applied to the membrane are observed. Discrete values of  $P$  can be determined at given percentages of the water transfer. They increase with the partial pressure, especially at high relative pressures ( $P/P_0 \approx 0.8 - 1$ ). The evolution of the water permeability as a function of  $a_w$  has been related to the sorption mechanism. From a practical point of view, both Estane 58237 and Estane 58245 present an interesting breathable character, especially at high values of  $a_w$ . Nevertheless, this property is related to important values of the water uptake. It is also accompanied by a decrease in the apparent diffusion. To limit these phenomena, which could represent disadvantages for applications (notably with respect to the drying rates of these materials), the chemical modification of Estane 58245 is now envisioned.

The authors acknowledge Région Rhône Alpes for its financial support and a grant to N. Dolmaire, and they also acknowledge Service RMN, especially M. F. Llauro from the Fédération de Recherche des Polyméristes Lyonnais FR2151, for the NMR analysis of TPU.

## REFERENCES AND NOTES

1. Bohdanecky, M.; Petrick, S.; Hadobas, F.; Simek, L. *Makromol Chem Macromol Symp* 1992, **58**, 1.
2. Yilgör, I.; Yilgör, E. *Polymer* 1999, **40**, 5575.
3. Kanapitsas, A.; Pissis, P.; Ribeles, J. L. G.; Pradas, M. M.; Privalko, V. *J Appl Polym Sci* 1999, **71**, 1209.
4. Petrik, S.; Hadobas, F.; Simek, L.; Bohdanecky, M. *J Appl Polym Sci* 1993, **47**, 677.
5. Green, R. J.; Corneillie, S.; Davies, J.; Davies, M. C.; Roberts, C. J.; Schacht, E.; Tandler, S. J. B.; Williams, P. M. *Langmuir* 2000, **16**, 2744.
6. Petrik, S.; Hadobas, F.; Simek, L.; Bohdanecky, M. *Eur Polym J* 1992, **28**, 15.
7. Schneider, N. S.; Illinger, J. L.; Karasz, F. E. *J Appl Polym Sci* 1993, **47**, 1419.
8. Barrie, J. A. In *Diffusion in Polymers*; Crank, J.; Park, G. S., Eds.; Academic: London, 1968; p 259.
9. Brunauer, S.; Emmett, P. H.; Teller, E. *J Am Chem Soc* 1938, **60**, 309.
10. Starkweather, H. W. In *Water in Polymers*; Rowland, S. P.; Ed.; American Chemical Society: Washington, DC, 1980; p 433.
11. Despond, S.; Espuche, E.; Domard, A. *J Polym Sci Part B: Polym Phys* 2001, **39**, 3114.
12. Camberlin, Y.; Pascault, J. P.; Letoffe', M.; Claudy, P. *J Polym Sci Polym Chem Ed* 1982, **20**, 383.
13. Vatalis, A. S.; Kehayoglou, H. *J Macromol Sci Pure Appl Chem* 2001, **38**, 673.
14. Cuve', L.; Pascault, J. P.; Boiteux, G.; Seytre, G. *Polymer* 1991, **32**, 343.
15. Crank, J. *The Mathematics of Diffusion*; Oxford University Press: London, 1975.

16. Zhang, Z.; Britt, I. J.; Tung, M. A. *J Polym Sci Part B: Polym Phys* 1999, **37**, 691.
17. Ree, M.; Han, H.; Gryte, C. C. *J Polym Sci Part B: Polym Phys* 1995, **33**, 505.
18. Paul, D. R. *Macromol Symp* 1999, **138**, 13.
19. Detallante, V. Thesis, University of Rouen, 2002.
20. Marais, S.; Hirata, Y.; Langevin, D.; Chappey, C.; Nguyen, T. Q.; Metayer, M. *Mater Res Innovations* 2002, **6**, 79–88.
21. Brunauer, S. *The Adsorption of Gases and Vapours*; Princeton University Press: Princeton, NJ, 1943.
22. Schneider, N.; Dusablon, L.; Snell, E.; Prosser, R. *J Macromol Sci Phys* 1969, **3**, 623.
23. Schneider, N.; Langlois, D.; Byrne, C. *Polym Mater Sci Eng* 1993, **69**, 249.
24. Flory, P. J. *Principles of Polymer Chemistry*; Cornell University Press: Ithaca, NY, 1953.
25. Water in Polymers; Rowland, S. P., Ed.; *ACS Symposium Series 127*; American Chemical Society: Washington, DC, 1980.
26. Zimm, B. H.; Lundberg, J. L. *J Chem Phys* 1956, **60**, 425.
27. Anderson, R. B. *J Am Chem Soc* 1946, **68**, 686.
28. De Boer, J. H. *The Dynamical Character of Adsorption*, 2nd ed.; Clarendon: Oxford, 1968.
29. Guggenheim, E. A. *Applications of Statistical Mechanics*; Clarendon: Oxford, 1966; p 186.
30. Taoukis, P. S.; Meskine, A. E.; Labuza, T. P. In *Food and Packaging Interactions*; Hotchkiss, J. H., Ed.; American Chemical Society: Washington, DC, 1988; p 244.
31. Jonquière, A.; Fane, A. *J Appl Polym Sci* 1998, **67**, 1415.
32. Koningsveld, R.; Kleinjens, L. A. *Macromolecules* 1971, **4**, 637.
33. Favre, E.; Schaetzel, P.; Nguyen, Q. T.; Clément, R.; Néel, J. *J Membr Sci* 1994, **92**, 169.
34. Pissis, P.; Apekis, L.; Christodoulides, C.; Niaounakis, M.; Kyritsis, A.; Nedbal, J. *J Polym Sci Part B: Polym Phys* 1996, **34**, 1529.